RSeeds: Rigid seeding method for studying heterogeneous crystal nucleation

Tianmu Yuan,[†,‡] Ryan S. DeFever,[†] Jiarun Zhou,[†] Ernesto Carlos Cortes-Morales,[¶] and Sapna Sarupria[*,¶]

[†]*Department of Chemical and Biomolecular Engineering, Clemson University, Clemson, South Carolina 29634, USA*

[‡]*Department of Chemical Engineering, The University of Manchester, Manchester, UK, M13 9PL*

[¶]*Department of Chemistry, University of Minnesota Twin Cities, Minneapolis, Minnesota 55455, USA*

E-mail: sarupria@umn.edu

Abstract

Heterogeneous nucleation is the dominant form of liquid-to-solid transition in nature. Although molecular simulations are most uniquely suited to study nucleation, the waiting time to observe even a single nucleation event can easily exceed current computational capabilities. Therefore, there exists an imminent need for methods that enable computationally fast and feasible studies of heterogeneous nucleation. Seeding is a technique that has proven successful at dramatically expanding the range of computationally accessible nucleation rates in simulation studies of homogeneous crystal nucleation. In this paper, we introduce a new seeding method for heterogeneous nucleation called Rigid Seeding (RSeeds). Crystalline seeds are treated as pseudo-rigid bodies and simulated on a surface with metastable liquid

above its melting temperature. This allows the seeds to adapt to the surface and identify favorable seed–surface configurations, which is necessary for reliable predictions of crystal polymorphs that form and the corresponding heterogeneous nucleation rates. We demonstrate and validate RSeeds for heterogeneous ice nucleation on a flexible self-assembled monolayer surface, a mineral surface based on kaolinite, and two model surfaces. RSeeds predicts the correct ice polymorph, exposed crystal plane, and rotation on the surface. RSeeds is semiquantitative and can be used to estimate the critical nucleus size and nucleation rate when combined with classical nucleation theory. We demonstrate that RSeeds can be used to evaluate nucleation rates spanning many orders of magnitude.

Introduction

Heterogeneous nucleation plays an important role in all liquid-to-solid transitions and thus, has wide relevance from pharmaceuticals to atmospheric science. The combination of lengthscales (∼nm) and timescales (∼ns) associated with the formation of nascent nuclei is difficult to probe experimentally. Thus, molecular simulations have played a substantial role in developing our understanding of this process in both bulk homogeneous and heterogeneous environments.

One of the most studied heterogeneous nucleation processes is the transition of liquid water to ice. Ice nucleation plays important roles in many facets of life, from cloud formation[1,2] and snowfall,[3] to cryopreservation[4,5] and food preservation.[6] Pure liquid water at atmospheric pressure is metastable up to nearly 40 K below the melting point of ice.[7] Therefore, nearly all ice nucleation in nature is heterogeneous – i.e., it occurs at the surface of some foreign particle. However, despite its omnipresence, the causal relationship between surface properties and ice nucleation propensity remains to be elucidated.

Computational studies have investigated heterogeneous ice nucleation on a range of surfaces, from minerals such as AgI,[8–11] mica[12–14] and kaolinite[15–19] to organic monolayers[20] and crystals,[21,22] graphite,[23–25] and simple model surfaces.[26–29] Despite these recent

studies, systematic evaluation of heterogeneous ice nucleation in molecular simulations remains challenging. Current computational power practically limits ice nucleation in straightforward molecular dynamics (MD) simulations[1] to conditions where the nucleation rate[2] falls roughly between 10^{28} $m^{-3}s^{-1}$ – 10^{33} $m^{-3}s^{-1}$. Under homogeneous conditions, this five orders of magnitude difference in nucleation rate correspond to a difference of no more than 5 K supercooling.[30] Even with coarse-grained models of water such as the mW model,[31] the range of computationally accessible conditions is minimally expanded, by perhaps 1 or 2 orders of magnitude in the nucleation rate. This constraint severely limits the range of surfaces and conditions for which straightforward MD simulations can be used to study heterogeneous ice nucleation.

Advanced sampling methods substantially increase the range of conditions that can be studied with MD simulations. Umbrella sampling,[32] metadynamics,[33,34] aimless shooting transition path sampling,[35–37] and forward flux sampling[38–40] (FFS) have been applied to study ice nucleation.[16,23,41–43] Umbrella sampling and metadynamics are free energy methods which allow for estimation of the nucleation barrier (and indirectly, the nucleation rate),[42] while FFS and aimless shooting are path sampling methods which generate an ensemble of transition paths[35,36,38,39] which can be used to investigate the mechanism and search for the reaction coordinate[35,36,44] of ice nucleation.[24,43,45–47] Importantly, FFS also allows for simple and direct evaluation of the nucleation rate.[38–40,47]

Though these advanced sampling methods dramatically expand the range of accessible nucleation conditions and rates, they each have their limitations. The free energy methods require a good order parameter, i.e., one which closely approximates the true reaction coordinate. This is difficult to know *a priori*, particularly in the case of heterogeneous nucleation, where the reaction coordinate could be affected by the specific surface. Furthermore, advanced sampling methods are computationally expensive.[3] In the ex-

[1]With straightforward molecular dynamics (MD) simulations we mean brute force simulations in which no enhanced sampling methods or rare event techniques have been used.

[2]Assuming a system of 10,000 water molecules, with a lower bound on the nucleation time of 1 ns and an upper bound of 100 μs.

[3]This observation is not a criticism of the methods but rather a comment on the difficulty of studying

treme example, using FFS to evaluate the homogeneous ice nucleation rate at a single condition for a molecular model of water (TIP4P/Ice)[48] required 22 million CPU-hours.[49] Clearly other methods are necessary to rapidly evaluate ice nucleation across a wide range of surfaces at the scale necessary to screen hundreds of surfaces for their ice nucleating propensity, and ultimately, engineer surfaces with desired ice nucleation properties.

Seeding[50–53] is an approach that widely expands the range of accessible nucleation conditions for homogeneous crystal nucleation. A crystalline embryo (seed) is carefully equilibrated in a bath of liquid. After equilibration, a straightforward MD simulation is performed. Given sufficient time, the seed will either dissociate or grow until the entire system becomes solid. The seed size that has a 50% chance of growth is the critical nucleus size at the temperature of the simulation. The free energy of forming the critical nucleus can be calculated by combining the critical nucleus size with the free energy difference between the bulk liquid and solid phases. The final information necessary to estimate the nucleation rate is the kinetic prefactor; this is estimated by extracting nuclei growth and dissociation rates near the critical size.

Homogeneous seeding has been used to evaluate nucleation rates spanning *nearly 200 orders of magnitude.*[54] It is thus a powerful method for evaluating nucleation under a wide range of conditions.[55,56] Given this strength, it would be beneficial to apply seeding to studies of heterogeneous nucleation. However, seeding has challenges. The numerical estimate of the free energy barrier is particularly sensitive to the definition of the critical nucleus size.[53] The nucleation rate is proportional to the exponential of the free energy barrier, making the estimated rate more susceptible to the exact definition of the nucleus size. Fortunately, for the purposes of comparing *relative* nucleation rates using the same definition of crystal nucleus size, this is less problematic.

Applying seeding to heterogeneous systems drastically complicates the situation. Myriad new challenges arise, such as identifying the crystalline plane that should be in contact with the surface, the rotation of the seed on the surface, the seed–surface contact

ice nucleation in molecular simulations.

angle, and, identifying if the solid molecules near the surface even adopt a typical crystalline structure, or instead they adapt to the surface with some intermediate structure between the structure of the bulk crystal and surface. Recently, a method called heterogeneous seeding (HSEED)[57] was devised to address these challenges and extend the seeding method to heterogeneous systems. HSEED is similar to homogeneous seeding but addresses the additional requirement of identifying the structure of the surface–seed interface. Hemispherical caps are generated from the crystal structure with different crystalline planes exposed on the side of the seed which will be placed in contact with the surface. A random structure search is performed to identify promising seed–surface configurations. Various surface–seed configurations are generated by rotating and translating the seed on the surface. For each, every water molecule within the first contact layer of the surface is perturbed through small random rotations and translations. Roughly 10^3 – 10^4 seed–surface configurations are generated for each surface/crystal plane combination. Each configuration is then energy minimized. The three lowest-energy seed–surface configurations are selected for each surface/crystal plane combination and solvated. After this step, the procedure closely resembles homogeneous seeding. Several MD simulations are initiated from each solvated configuration. Following an equilibration procedure, each system is simulated at the production temperature until the seed grows or dissociates. For low temperatures and/or large seeds all crystal planes may grow. However, there should be a temperature/seed size where only seeds with a single specific crystal plane exposed to the surface grow. This plane is the most favorable crystal plane for ice nucleation on the given surface.

HSEED successfully identified the correct ice crystal plane (in comparison to results from metadynamics) at the seed–surface interface with two different model surfaces and the mW water model. When tested with the all-atom TIP4P/Ice model and an organic surface, HSEED once again identified the correct crystal plane (compared to results from FFS). HSEED requires roughly one order of magnitude fewer computational resources compared with metadynamics or FFS[57] which makes HSEED a promising method to ex-

plore heterogeneous crystal nucleation on a range of surfaces. However, the interfacial ice structure predicted by HSEED on a model surface did not fully agree with their metadynamics results, suggesting that the random structure search may have challenges on rougher and non-uniform surfaces. In addition, there are some discrepancies between the critical nucleus size estimated by HSEED and metadynamics. We propose an alternative seeding method that can potentially overcome the above limitations.

We introduce a new method called Rigid Seeding (RSeeds). Favorable surface–seed configurations are identified by treating the ice seeds as pseudo-rigid bodies and simulating them on a surface with liquid water above the melting temperature. Since they are treated as pseudo-rigid bodies, the seeds cannot dissociate. However, they can rotate and translate on the surface to identify favorable seed–surface configurations. Some liquid water is left between the surface and seed to allow for structure intermediate between the surface and ice seed to bridge the two. Following an annealing and equilibration procedure to bring the system temperature to the desired production temperature below the melting point, the ice seeds are no longer treated as rigid bodies. The systems are then allowed to evolve to determine the seeds which grow and dissociate. RSeeds is developed and tested for heterogeneous ice nucleation, but the ideas presented here should be easily extended to other types of heterogeneous crystal nucleation.

In the remainder of the paper, we describe the RSeeds method in detail and demonstrate the method on two realistic surfaces, and on the model surfaces studied in Ref.[58] We discuss the role of interfacial water in determining nucleation behavior. We also demonstrate that nucleation rates can be determined by combining critical nucleus size determined using RSeeds, and classical nucleation theory.

Methods

Description of the RSeeds method

A schematic of the RSeeds method is shown in Fig. 1 and details of each step are discussed below. The RSeeds method involves placing rigid ice seeds on a surface with interfacial water, performing equilibration to relax the interfacial water molecules (crystal–liquid, liquid–surface, and crystal–surface) followed by a production run where the ice seed is no longer rigid to evaluate the fate of the seed on the surface. The process involves four steps (1-4). Details of each step are provided below.

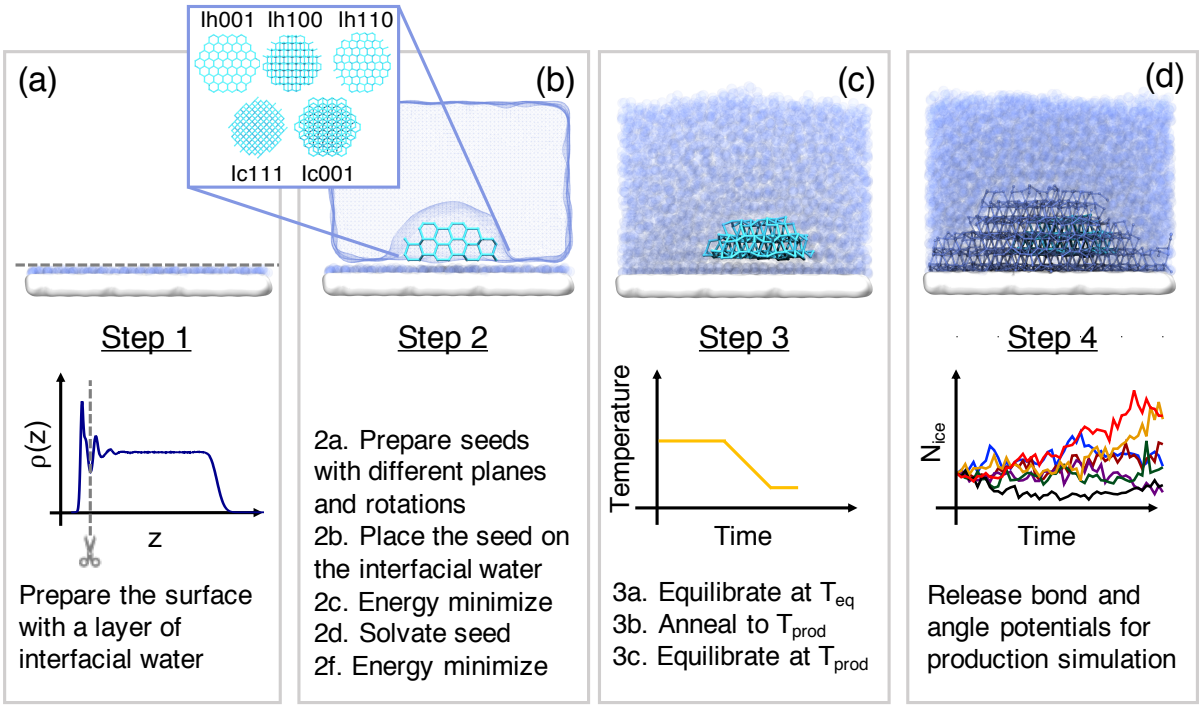

Figure 1: Schematic of the RSeeds method. Steps 1–4 are shown in panels (a)–(d), respectively. A generic surface is shown in white. Liquid water, ice seeds, and growing ice are shown as light purple spheres, cyan bonds, and dark purple bonds, respectively. N_{ice}: largest cluster of ice-like molecules; $\rho(z)$: density of water normal to the surface; z: distance normal to the surface; T_{eq}: Equilibration temperature; T_{prod}: Production temperature.

Surface Preparation (Step 1)

The goal of this step is to generate a surface with interfacial water molecules upon which the rigid ice seed will be placed (see Fig. 1(a)). We begin with simulations of a liquid water slab on the surface at equilibration temperature (T_{eq}). This equilibrates the surface under aqueous conditions and provides an interfacial water configuration. The water slab should be thick enough that the interfacial water structure at the surface is not dependent upon the thickness of the slab. T_{eq} is chosen to be above the melting temperature to help the system equilibrate within a few nanoseconds. We choose T_{eq} as 300 K. Once the system is equilibrated, the water molecules within a specified distance of the surface are retained with the surface, while all other water molecules are removed. This specified distance usually corresponds to one or two hydration layers as determined by the water density along the surface normal ($\rho(z)$). In the results presented here, the distance corresponds to the first minimum in $\rho(z)$ (i.e., first hydration layer), and the equilibration runs were 5 ns. The snapshot in Fig. 1(a) shows the system after retaining water molecules in the first hydration layer. The amount of interfacial water required is likely to be surface dependent. Surfaces with more roughness, surface ions, or water penetration, may require a thicker interfacial water layer.

Rigid seed placement (Step 2)

The goal of this step is to generate and place ice seeds on the surface–interfacial water system prepared in Step 1 (see Fig. 1(b)). The ice seeds are cut from a perfect ice crystal. Different crystal polymorphs, surface-exposed crystal planes, and rotations of the seed on the surface may need to be tested. Since ice formation on surfaces has been shown to nucleate through both the hexagonal (Ih) and cubic (Ic) polymorphs of ice[8,9,15–18,20,21,23,24,26–29,45,57,59–66] under atmospheric conditions, both crystals are tested. For large seeds, stacking-disordered ice could also be tested. For each ice polymorph, there exist many crystal planes which could be exposed to the surface. We limit our search to

seed caps with low Miller index planes exposed on the "surface side" of the seed cap, as these are expected to be more stable. Hemispherical caps are used if there is no prior knowledge of the ice–surface contact angle. We tested a total of five ice planes: Ih basal plane (Ih001), Ih primary prismatic plane (Ih100), Ih secondary prismatic plane (Ih110), Ic 001 plane (Ic001), and Ic 111 plane (Ic111), shown in Fig. 1(b). The seeds are referred to based on the initial plane parallel to the surface.

Once the ice seeds have been created (Step 2a), "artificial" harmonic bond and angle potentials are added between each oxygen in the seed and all of its first neighbor oxygen atoms. The cutoff distance used to determine the first neighbor is 0.33 nm, which results in four first neighbors for each oxygen atom in the bulk environment. Oxygen atoms near the surface of the seed will have fewer first neighbors. Oxygen atoms with four first neighbors participate in four bonds each and are the central atom (i.e., atom a_j of angle a_i–a_j–a_k) in six angles. Force constants for the bond and angle potentials are selected to reproduce the bond and angle distributions in ice. This ensures that the seed does not deform at T_{eq}. Note that the hydrogen positions are not restrained; water molecules are free to rotate and change hydrogen-bonding patterns both within the seed and between the seed and surrounding water molecules.

To sample the different orientations the seed can take relative to the surface, we place the seed at different rotations. If the surface-exposed plane is rotationally symmetric for 180° (Ic001, Ih100, and Ih110), 3 different rotations (i.e., 0°, 60°, 120°) are required. Since Ih001 and Ic111 are rotationally symmetric for 60°, only one configuration is required for each. We find this increment sufficient as seeds rotate up to ∼30° during the equilibration at T_{eq}. The results are not sensitive to the precise x, y placement of the seeds because the seeds are free to translate on the surface during the equilibration at T_{eq}, and the surfaces in this work have relatively small repeating units of pattern. On surfaces with larger lengthscale features or greater surface heterogeneity, seeds with different initial x, y placement may need to be tested. The z position of the seed is selected to minimize the vacuum space between the seed and the interfacial water layer while preventing atomic

overlaps (Step 2c). An energy minimization (Step 2d) is performed after the seed is placed on the interfacial water layer.

A separate simulation is performed to equilibrate liquid water at T_{eq}. The x and y dimensions of this system are the same as those of the surface. The z dimension is at least 2 nm larger than the z dimension of the hemispherical seed caps. The final water configuration from this simulation is used to solvate the surface–seed system (Step 2e). Water molecules that overlap with the seed are removed. Energy minimization (Step 2f) is performed to relax the seed–water interface. At the end of Step 2, the system is composed of a surface, a layer of interfacial water, and a solvated rigid seed (Fig. 1(b)). The remaining steps of the method are performed with three independent trajectories for each constructed configuration.

Equilibration and Annealing (Step 3)

In this step, the systems generated in Step 2 are subjected to annealing and equilibration (see Fig. 1(c)). Each system is equilibrated at T_{eq} for 10 ns (Step 3a). This step relaxes the seed–water, surface–water, and seed–surface interfaces. While the bond and angle potentials prevent the rigid seed from dissociating, it is free to translate and rotate on the surface. We find that seeds rotate up to $\sim 30^{\circ}$ on the surface for the seed sizes we tested ($\leq$ 450 water molecules). Larger seed sizes may rotate less and thus require finer increments of rotation when placing seeds on the surface in Step 2. Some seeds tilt such that the surface-exposed crystal plane changes, or even translate away from the surface. Further discussion is provided in Sec. Results and discussion. Following equilibration at T_{eq}, the system is annealed from T_{eq} to the target temperature, T_{prod}. A final equilibration is performed at T_{prod} before the production simulation to ensure that the system is equilibrated at T_{prod} (Step 3c). In the studies presented here, we have used T_{eq} to ensure that the water molecules and seed were able to sample different conformations effectively, however, it may be prudent to assess the effect of T_{eq} on the outcome of the seeding process.

Production simulations (Step 4)

This step comprises the simulations performed to determine if the seed grows or dissociates on the surface. The bond and angle potentials preventing the seed from dissociating are removed prior to the start of the simulation. For TIP4P/Ice water model, the system is simulated for ∼50 ns depending on the dynamics at the production temperature, and for mW water model, the system either fully grows or dissociates within 2.5 ns. The following information can be combined to assess ice nucleation on a surface: (1) the crystal polymorph, and ice plane in contact with the surface at the start of the production simulation, (2) the size of the seed at the start of the production simulation, and (3) the change in the seed size during the production simulation.

Generation of the surfaces used in the simulations

RSeeds was tested with four surfaces: a self-assembled monolayer (SAM) with COOH terminal group, a model surface that closely mimics the mineral kaolinite (kao_m), and two model FCC surfaces (s1 and s2) constructed from Ref. 28.

Flexible COOH SAM surface

SAM surfaces are flexible organic surfaces composed of alkane chains attached to a metal surface. In our simulations, each SAM chain consists of a sulfur head group connected to a 10-carbon alkane-chain spacer, and a terminal –COOH functional group (S-$(CH_2)_{10}$-COOH). The position of the sulfur head group is restrained to mimic the alkanethiolates supported on metal surfaces. With the exception of partial charges, all bonded and non-bonded parameters were taken from the General Amber[67] force field. Partial charges were taken from the OPLS-AA[68] force field.

To validate our model, we compared SAM tilt and twist angles and the contact angle of water on the surface with experimental values. For these calculations, the sulfur atoms were restrained in the positions they would occupy if adsorbed on an Au(111) surface. The

in-plane structure of the sulfur atoms was $\sqrt{3}\times\sqrt{3}$R30° with a 0.497 nm distance between neighboring sulfur atoms.[69] The model surface predicts a tilt angle of 32° and a twist angle of 46° at 300 K compared with experimental values of 28° and 53°, respectively.[69] The experimental measure for the water contact angle[70] is <10° and we observe water completely wets the surface.

The COOH SAM surface used to test RSeeds had a spacing of 0.45 nm between neighboring sulfur groups instead of 0.497 nm. This results in a 0% lattice mismatch to the hexagonal unit cell of ice.[20] The tilt and twist angles in this setup are 2° and 84°, respectively. The COOH SAM surface was 8.1 × 7.8 nm^2 in the $x-y$ dimensions and consisted of 360 SAM chains.

Mineral surface, kao$_\mathrm{m}$

Kao$_\mathrm{m}$ is a model surface that closely mimics the crystal structure of kaolinite. Complete details of the kao$_\mathrm{m}$ surface construction are provided in the Supporting Information. Surface atoms except for the hydrogen of the surface hydroxyl groups were held fixed for all simulations. Non-bonded parameters for the surface were taken from the CLAYFF[71] force field. A 6×6×11 nm^3 and a 14×14×14 nm^3 box were created with 2 mirrored kao$_\mathrm{m}$ surfaces with ∼7 nm and ∼10 nm vacuum space between the two surfaces, respectively. The simulation setup is similar to that described in Ref. 18. The surfaces are periodic in x and y and placed such that there is 1 nm between the surface and the box boundaries in z.

MD simulation details

MD simulations with TIP4P/Ice water model[48] were carried out using the GROMACS[72] 2018 simulation package. The timestep was set to 2 fs and the equations of motion were integrated with the Leap-Frog algorithm. The Lennard Jones and short-range electrostatic cutoffs were set to 1.0 nm. Long-range electrostatic interactions were evaluated

using Particle Mesh Ewald[73] method. The geometry of water molecules was maintained with the SETTLE algorithm,[74] with the exception of water molecules in the rigid seed, which was constrained using the LINCS[75] algorithm. Software limitations were the only reason for this choice – GROMACS does not allow SETTLE to be applied to multiple different molecule types. Simulations with mW water model[31] were carried out using the LAMMPS[76] simulation package, and the equations of motion were integrated with velocity Verlet algorithm and the timestep was set to 5 fs. The Lennard Jones cutoff was set to be three times the sigma value.

All simulations including a surface were performed in the NVT ensemble. The Bussi thermostat[77] was used to maintain temperature. Though simulations were performed in the NVT ensemble, the vacuum space above the water slab acts as a natural barostat, maintaining pressure at $\sim$0 bar. Equilibration simulations of bulk liquid water and ice were performed in the NpT ensemble at $p = 0$ bar with the Bussi thermostat[77] and Berendsen barostat.[78] Production simulations of bulk liquid water and ice were performed in the NVT ensemble with the Bussi thermostat.

Order parameter

The evolution of the size of the largest ice cluster is monitored throughout the simulation. The neighbor averaged $\overline{q}_6$ order parameter developed by Lechner and Dellago is used to classify the water molecules as solid or liquid for TIP4P/Ice.[79] The cutoff distance to identify neighbors of oxygen atoms was set to 0.35 nm. If $\overline{q}_6 > 0.358$, the water molecule is classified as a solid, otherwise it is a liquid.[80] The q_3 order parameter developed by Li et al.[41] is used for mW water model. The cutoff distance is 0.34 nm to identify the neighbor oxygen atoms, and the particle will be characterized as solid if $q_3 < -0.69$. We calculate the largest cluster size of connected solid water molecules to evaluate the growth or dissociation of the seed.

Results and discussion

We test and validate RSeeds on four surfaces: a flexible SAM surface with COOH terminal groups (COOH), a modified mineral surface based on kaolinite (kao_m), and two model FCC surfaces (s1 and s2). We compare the results obtained from RSeeds with those from straightforward MD simulations and metadynamics. We demonstrate that RSeeds is able to identify the ice polymorph as well as the ice–surface interface in all studies. Additionally, the critical nucleus size on the kao_m surface predicted from RSeeds is in good agreement with an estimate from straightforward MD simulations at 237.5 K and the predicted critical nucleus size on s1 and s2 surfaces are comparable with those reported from metadynamics at 235 K.[28] We obtain the nucleation rate for kao_m at 237.5 K from heterogeneous classical nucleation theory (CNT) by combining results from RSeeds with predictions from homogeneous seeding. The obtained nucleation rate compares favorably with an estimate from straightforward MD simulations. We caution readers that care must be taken in extending CNT to heterogeneous nucleation. If the ice polymorph formed on the surface is different from the polymorph in homogeneous nucleation, the potency factor, $f(\theta_c) = V_{het}/V_{hom}$, becomes ill-defined.[28]

Harmonic bond and angle potentials

Harmonic bond and angle potentials were applied between water oxygen atoms of neighboring water molecules in the crystalline seed to prevent the seed from dissociating in Steps 1–3. The choice of parameters for the bond and angle potentials (i.e., equilibrium bond length, equilibrium angle, and bond and angle force constants) depends on the water model and the simulation conditions. In this work, both mW and TIP4P/Ice water models are used at temperatures between ∼230 and 300 K and pressure of 0 bar. Since it is most important to reproduce the structure of ice at conditions close to our production conditions, we performed MD simulations of bulk Ih and Ic at 230 K and 0 bar to identify the parameters for the bond and angle potentials. Following equilibration in the

NpT ensemble, MD simulations of bulk Ic and Ih were performed at 230 K in the NVT ensemble. Distributions of the bond length, angle (θ), and dihedral angle (θ_d) between neighboring oxygen atoms for TIP4P/Ice are reported in Fig. 2. The bond length and angle with the highest probability were selected as the equilibrium bond length and angle for the harmonic potentials.

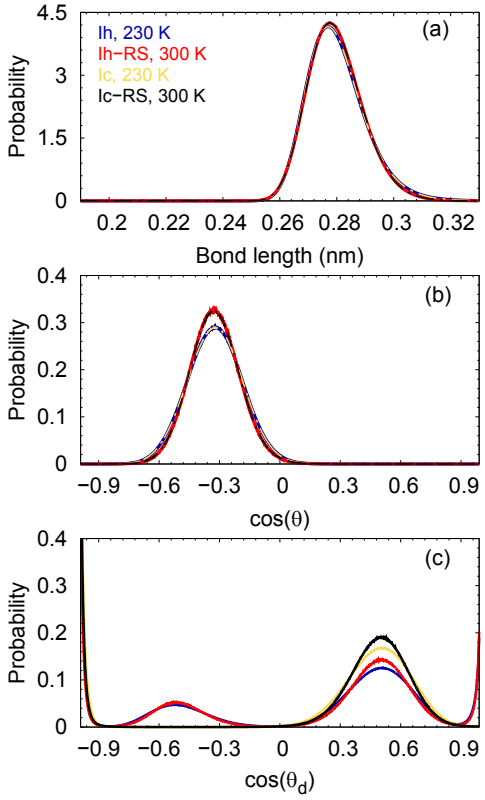

Figure 2: Oxygen–oxygen 'bond' length, angle, and dihedral angle probability distributions from bulk ice and rigid seeds for TIP4P/Ice. The bond length, angle (θ), and dihedral angle (θ_d) distribution are shown in panels (a)–(c), respectively. Ih-RS and Ic-RS denote rigid seeds of Ih and Ic, respectively.

The force constants for the harmonic bond and angle potential need to be sufficiently strong to maintain the structure of the ice seed under the highest simulation temperature and reproduce the bond, angle, and dihedral distributions found in ice as closely as possible. Spherical ice seeds with a radius of 1.5 nm were generated for both Ih and Ic. The seeds were solvated with a 6×6×6 nm^3 water box that is periodic in x, y, and z directions. The system was first equilibrated at 0 bar and T_{eq} in an NpT simulation, followed by

an NVT simulation at T_{eq}. A range of bond and angle force constants were tested. For every seed, the nearest neighbors of each water molecule are determined (based on the cut-off value obtained from the bulk ice structure). Bonds are defined between the central water molecule and the determined neighbors. The angles are obtained based on the bonds. Values that best reproduced the probability distributions for bonds, angles, and dihedrals in bulk ice polymorph simulations were selected as the force constants for the harmonic bond and angle potentials. Fig. 2 compares the distributions of bond lengths, angles, and dihedral angles obtained for the rigid seed at 300 K and bulk ice at 230 K for TIP4P/Ice. The equilibrium bond length and angle are 0.278 nm and 108.6°, and the force constants used are 7000 kJ mol^{-1} nm^{-2} and 20 kJ mol^{-1} $radian^{-2}$, respectively. For mW water model, we use 0.27 nm and 109.47° for the equilibrium bond length and angle. The force constants are 5 kcal mol^{-1} $Å^{-2}$ and 2 kcal mol^{-1} $radian^{-2}$ for bond and angle, respectively. Note that we keep all parameters of the water model the same and add the harmonic bond and angle potentials. Normally the non-bonded interactions (i.e., Lennard Jones and Coulombic) between 1–2 and 1–3 interactions are excluded when atoms are connected through bonds and angles, but in this case, we keep the non-bonded interactions between water molecules and manually exclude the non-bonded interactions within the water molecules. There are two reasons for this, the first one is to keep the hydrogen bonding network of the ice structure by allowing intermolecular interactions. The second reason is that the repulsive term from the Lennard Jones interactions assists the seed in retaining its structure. In the absence of this, the electrostatic interactions between oxygen and vicinal hydrogen atoms would disrupt the crystalline seed. It is possible to add dihedral angle potentials in addition to the bond and angle potentials to maintain the seed structure. Our results indicate that bond and angle potentials are sufficient to maintain the ice seed structure and reproduce the correct bond, angle, and dihedral distributions at T_{eq}.

Rigid seeding on COOH surface

Since we assume no prior knowledge of the ice polymorph or surface-exposed crystal plane that nucleates on the COOH surface, five seeds (Ih100, Ih110, Ih001, Ic001, Ic111) consisting of ∼250 water molecules are prepared. As described in Sec. Methods the rotational symmetry of the Ih110, Ih100, and Ic001 planes require three rotations (0°, 60°, 120°) each. Ih001 and Ic111 only require a single rotation, resulting in a total of 11 starting seed configurations. Three independent simulations are initiated from each configuration at the start of Step 3. T_{eq} and T_{prod} are 300 K and 250 K, respectively.

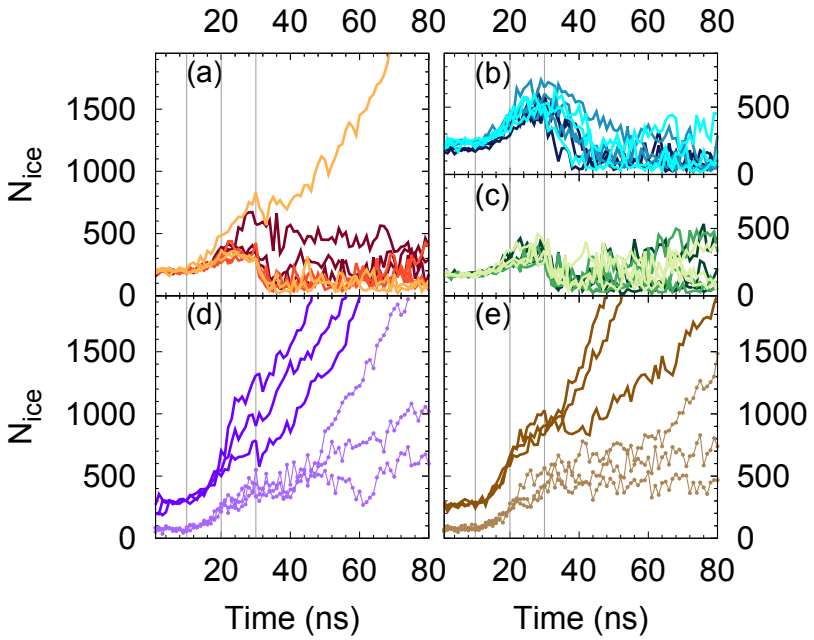

Figure 3: Number of molecules in the largest cluster of ice-like water molecules as a function of time on the COOH surface. Panels (a)–(e) correspond to the seeds with Ic001, Ih100, Ih110, Ic111, and Ih001 planes in contact with the surface, respectively. The vertical lines demarcate Step 3a (0–10 ns), Step 3b (10–20 ns), Step 3c (20–30 ns), and Step 4 (30–80 ns). Different colors in panels (a), (b) and (c) correspond to different rotations. For example, in Panel (b), dark blue is 0°; cyan is 60°; blue is 120°. In panels (d) and (e), the trajectories represented by thin lines with points start from a smaller rigid seed. The data is plotted every 1 ns.

Fig. 3 shows the size of the largest ice cluster in the system on the COOH surface. Panels (a) and (d) show Ic seeds while (b), (c), and (e) show Ih polymorphs. Different line shades represent different initial seed rotations. In the first 10 ns (Step 3a) the cluster

size remains constant. Since T_{eq} is above the melting temperature no ice grows from the seeds, but the artificial bond and angle potentials prevent the seeds from dissociating. During this step, the rigid seeds are free to translate and rotate on the surface to find a favorable position and rotation. The layer of water molecules between the seed and surface can also reorganize as necessary to bridge the surface and rigid seed. In most cases, the seed does not change its position or rotation after 3 ns of simulation at T_{eq}. In a few cases, the seed–surface interface is so unfavorable that the seed translates away from the surface into the bulk. Two of the nine Ic001 seeds tilt in Step 3a such that the plane exposed to the surface changes from Ic001 to Ic111. These seeds continue to move (rotate/adjust) throughout Step 3a as well as in Step 3b. Snapshots of one of the seeds which tilted from Ic001 to Ic111 are shown in Fig. 4. Ice formed underneath the rigid seed during Step 3 and bridged the rigid seed structure to the surface in a configuration favorable for growth in Step 4. Portions of the rigid seed which were furthest from the surface (see Fig. 4(e)) even dissociated once the harmonic bond and angle potentials were removed, bu .

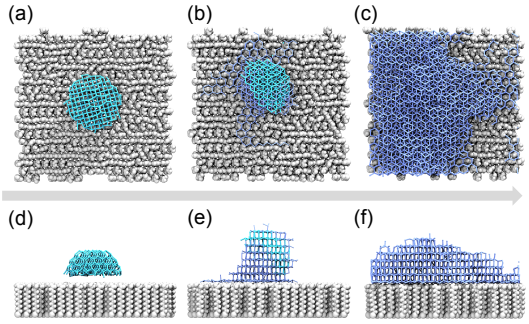

Figure 4: Snapshots of an Ic001 seed on COOH surface. The seed tilted to expose Ic111 to the surface. Panel (a)–(c) show the top-down view and (d)–(f) show the side view of the system at the end of Steps 2, 3, and 4, respectively. The rigid seed is shown as cyan bonds. Ice blue bonds show the cluster of ice-like water molecules. Liquid water is omitted for clarity.

During Step 3b, ice cluster growth is observed even under relatively mild supercooling. Water molecules in the rigid ice seed are restrained and thus effectively template ice growth. The number of water molecules in the largest ice cluster increases most for the

Ih001 (Fig. 3(e)) and Ic111 (Fig. 3(d)) seeds. Similar behavior is also observed for the two Ic001 seeds that tilted (Fig. 3(a)) to Ic111. This phenomenon continues in Step 3c; seeds with the Ih001 or Ic111 plane exposed to the surface continue growing while the other planes do not show significant growth. Unsurprisingly, the seeds that show the most growth during Step 3 continue to grow in Step 4, while the other seeds dissociate once the harmonic bond and angle potentials are removed. Of the two Ic001 seeds that tilted to Ic111, one grew and the other dissociated in Step 4 (Fig. 3(a)). Visualization of the two trajectories revealed that one of the seeds in Step 4 remained close to the surface and grew (see Fig. 4). The other seed translates further from the surface during Step 3c and dissociated after the harmonic bond and angle potentials were released in Step 4. Given the homogeneous critical nucleus size for TIP4P/Ice at 252.5 K (3167 water molecules),[81] this finding was unsurprising.

Based on the observations presented above, it appears that Ih001 and Ic111 are the favorable polymorph/crystal planes for ice nucleation on the COOH surface. However, since the sizes of the largest ice cluster in the system are not the same when the harmonic bond and angle potentials are removed (i.e., at the start of Step 4), these observations do not confirm with certainty that Ih001 and Ic111 are most favorable. We thus prepare two new seeds of Ih001 and Ic111 with a smaller size of 90 water molecules. The goal is to ensure that the ice cluster sizes at the start of Step 4 will be comparable to, or smaller than, the cluster sizes for the polymorphs/planes that dissociated. If Ih001 and Ic111 still grow under such conditions then these polymorphs/planes are definitively favored. Results for the two smaller seeds are shown as the thin lines with points in Fig. 3(d) and 3(e). For seed sizes in a range of 300–500 water molecules, only the seeds with planes of Ic111 and Ih001 exposed to the surface are able to grow. This indicates that Ih001 and Ic111 are indeed the favorable polymorph/planes for ice nucleation on the COOH surface. Ih001 and Ic111 are structurally similar and therefore, it is not surprising that if the surface and the corresponding interfacial water layer can support Ih001 it can also favor Ic111 (and vice versa). Thus, we observe both Ih001 and Ic111 growing on COOH

surface.

In order to test the validity of these predictions, we performed 13 straightforward MD simulations at temperatures between 240 K and 250 K. All simulations nucleated ice within 1 μs. We observed nucleation and growth of Ih001, Ic111, or stacking-disordered ice (Isd) in all cases. Although no Isd seeds were explicitly tested with RSeeds we did observe the formation of Isd in some cases as the seeds grew. These results indicate that the ice polymorph/crystal plane predictions from RSeeds are correct.

Rigid seeding on $\mathbf{kao_m}$ surface

RSeeds was also performed on $\mathrm{kao_m}$ surface. The same five ice planes (Ih100, Ih110, Ih001, Ic001, Ic111) and the necessary rotations were used, once again resulting in 11 different initial seed–surface configurations (Step 2). Two different production temperatures 240 and 252.5 K were used. Seed sizes of ∼160 water molecules are used for $\mathrm{T_{prod}}$ = 240 K, and ∼450 for 252.5 K. $\mathrm{T_{eq}}$ is chosen at 300 K for both cases. Results corresponding to 240 K are shown in Fig. 5(a)–(e). The Ih100 and Ih110 planes show growth in Steps 3b and 3c. These seeds continued to grow during Step 4. Visual inspection of the trajectories revealed that the two Ih110 seeds that grew most during Step 3a–Step 4 tilted from Ih110 to Ih100. In the case of the single Ih110 seed that shows limited growth during Step 3 and moderate growth in Step 4, we observe that Ih100 grows from the Ih110 seed and Ih100 ultimately subsumes the original seed during Step 4. Therefore, all cases which show seed growth in Step 4 have the Ih100 plane exposed to the $\mathrm{kao_m}$ surface at 240 K. The results obtained at 252.5 K (shown in Fig. 5(f)–(j)) also indicate that Ih100 seeds are favored on the $\mathrm{kao_m}$ surface.

Since the ice clusters at the start of Step 4 were larger for Ih100 compared with any other ice polymorph/plane combination at 240 K, we again prepare a smaller initial Ih100 seed (87 water molecules) to confirm that Ih100 is indeed favored over other possibilities. Results are reported as (gray) thin lines with points in Fig. 5(d). The smallest seed size

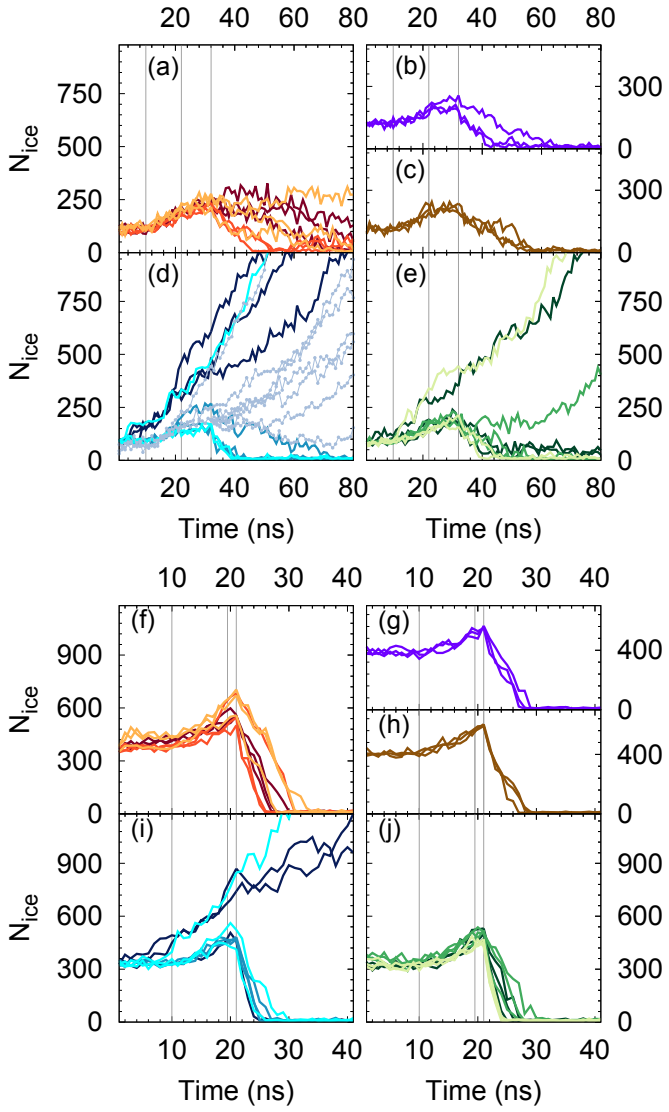

Figure 5: Number of molecules in the largest cluster of ice-like water molecules as a function of time on kao_m surface. Panel (a)–(e) correspond to the seed with Ic001, Ic111, Ih001, Ih100, and Ih110 planes, respectively, at T_{prod}=240 K. The vertical lines demarcate Step 3a (0–10 ns), Step 3b (10–22 ns), Step 3c (22–32 ns), and Step 4 (32–82 ns). Panel (f)–(j) correspond to the seed with Ic001, Ic111, Ih001, Ih100, and Ih110 planes, respectively, at T_{prod}=252.5 K. The vertical lines demarcate Step 3a (0–10 ns), Step 3b (10–18.5 ns), Step 3c (18.5–21 ns), and Step 4 (21–41 ns). Different colors in panel (a), (d), (e), (f), (i) and (j) correspond to different seed rotations. Thin gray lines with points in panel (d) start with a smaller rigid seed. The color for each ice plane is the same as COOH results. The data is plotted every 1 ns.

at the start of the production runs (Step 4) is 191 water molecules. This is comparable to the seed sizes obtained for other possibilities. Five independent simulations are initiated from this configuration. During the production simulation, four definitively grow and one neither grows nor dissociates. No other polymorph/crystal plane shows any growth with comparable seed size. As for 252.5 K, we found the critical nucleus size for Ih100 seed on kao_m surface to be 475 water molecules (see Sec.Critical nucleus size and nucleation rate estimates from RSeeds) which are smaller than any other planes of ice tested at the same temperature.

Besides the planes, there is also a preference in the rotation for the Ih100 plane on kao_m surface (see Fig. 6). From the RSeeds results, we note that all growth trajectories have Ih100 plane in contact with the kao_m surface with a certain orientation. More specifically, they have a $\sim 30^\circ$ angle (θ_r) between the c-axis of Ih and the y-axis of the surface. At 240 K, the starting seed configurations for Ih100 seed have $\theta_r = 0^\circ, 60^\circ$, and 120° as shown in Fig. 6(a)–6(c), respectively. The smaller initial Ih100 seed starts with $\theta_r = 0^\circ$. From Fig. 5(d), all three seeds with a starting rotation of $\theta_r = 0^\circ$ (dark blue) find the positions and rotations that result in growth, while all three seeds with $\theta_r = 120^\circ$ starting rotations (blue) shrink in the production run. One of three seeds with a starting $\theta_r = 60^\circ$ (cyan) grows in Step 4. This suggests that a 60° increment search is sufficient for seed sizes of $\sim$160 as the seed is able to rotate $\pm 30^\circ$ during Step 3. To further confirm this, we used a finer increment of the rotation and more independent trajectories to gather more statistics. We observed that there is a clear favorable rotation for Ih100 seed on kao_m and there are a large number of Ih110 seeds that tilt or translate away from the surface as we observed from the previous RSeeds results. Detailed results are provided in the Supporting Information. For a seed with $\sim$450 water molecules (see Fig. 5(i)), two out of three with $\theta_r = 0^\circ$ and one out of three with $\theta_r = 60^\circ$ grow during the production run. This indicates that the seeds with $\sim$450 water molecules are still able to rotate $\pm 30^\circ$, but it is worth noting that a finer increment may be required for a larger seed size. Fig. 6(d) shows the ice plane and rotation that the RSeeds method predicts and Fig. 6(f)

shows results obtained from straightforward MD simulation. A total of 11 nucleation trajectories are obtained using straightforward MD simulations at 240 K and 237.5 K. The ice polymorph, plane, and rotation obtained from RSeeds are in good agreement with results from straightforward MD simulations.

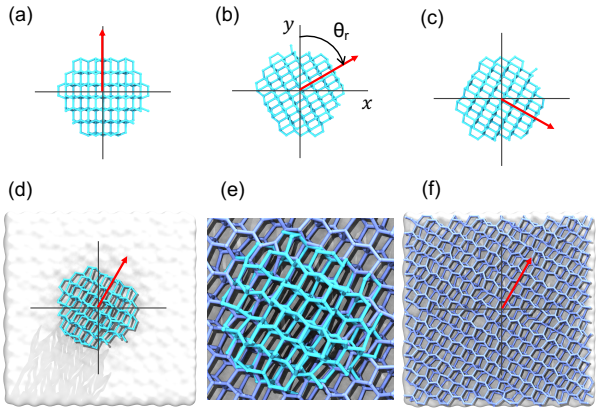

Figure 6: RSeeds method on kao_m (white) with Ih100 seeds (cyan) compared to ice from straightforward MD (purple). Panel (a)–(c) shows the 3 starting seed configurations with a θ_r of 0°, 60°, and 120°, respectively. (d) The ice configuration on the surface predicted by RSeeds. (e) The combination of RSeeds result and ice nucleated from straightforward MD. (f) The ice nucleated from straightforward MD. The surface is kept in the same orientation as indicated by the black lines (x- and y- axes), and the red arrow is the c-axis of the hexagonal ice, θ_r reported is the angle between the red arrow and the y-axis of the surface.

We also test the effect of initiating production simulations (i.e., Step 4) directly following Step 3b (i.e., without any equilibration at T_prod (Step 3c)). We find no effect on the final results with regards to the favorable ice polymorph, plane, and rotation provided the ice clusters are sufficiently large by the end of Step 3b. There are two main purposes for Step 3c. Firstly, this enables the system to equilibrate at T_prod before releasing the harmonic bond and angle potentials that hold the seed rigid. Secondly, since the seed is held rigid during Step 3c, a longer simulation leads to more growth of the seed, which allows us to explore a wider range of seed sizes at the start of Step 4. In principle, one could pick different seed sizes from various stages of Step 3c and use them to identify the critical nucleus size. However, there are certain caveats associated with this approach. There are differences in the growth rates between different planes and directions of ice seed, and a

longer simulation with a rigid seed may lead to an anisotropically shaped nucleus. It is certainly possible that some non-regular surfaces could have a critical nucleus size that is anisotropically shaped, but we emphasize that care must be taken if the shape of the nucleus before the production run is less regular. One of the solutions to this problem is to use a tunable potential as outlined by Sun *et al.*[82] The other solution is to pick a short annealing and equilibration time (Step 3b and 3c) so that the differences in growth rate no longer matter.

Rigid seeding on FCC surfaces

In order to compare the predicted ice plane and interfacial ice structure between HSEED and RSeeds, we performed RSeeds on both s1 and s2 surfaces with mW water model. To eliminate the finite size effects, both surfaces are 8×8 nm^2 in the x–y dimensions. Similar to the all-atom simulations, we used five ice planes with 60° rotational intervals which gave 11 initial seed–surface configurations (Step 2). A production temperature of 235 K is chosen to facilitate a direct comparison with HSEED[57] and metadynamics[28] results. A duration of 10 ns was used for equilibration at 300 K (Step 3a), 20 ps annealing (Step 3b), and 20 ps equilibration at 235 K (Step 3c). Due to the fast dynamics of mW water model, the duration of Steps 3b and 3c are significantly reduced to prevent the seed from rapidly growing. From our test results, it is also possible to eliminate Step 3b and quench the system down to the target temperature since the annealing time is short. In the end, it is the size of the largest cluster at the end of Step 3 that determines the fate of the system in the production run. RSeeds predicts that Ih001 and Ic111 are the favorable seeds on the s1 surface while Ih100 seeds are the most favorable on the s2 surface. These results agree with HSEED in terms of predicting the favorable ice planes on surfaces.

Several straightforward MD simulations were performed at 218 K for both surfaces. Simulations were performed at 218 K so that ice nucleation could observed within simulations times in straightforward MD. Although at different temperatures, the ice structures

obtained from straightforward MD at 218 K (shown in Fig. 7) are identical to metadynamics results at 235 K.[57] Snapshots of the system from the MD simulations at 218 K and RSeeds at 235 K are shown in Fig. 7. RSeeds is able to match the interfacial ice structure expected from the straightforward MD simulations for both s1 and s2 surfaces. This is extremely encouraging as the interfacial ice structure on the s2 surface does not resemble any common ice planes.

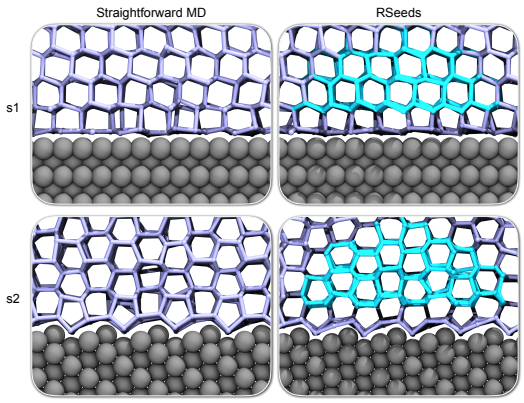

Figure 7: Snapshots of ice nucleating in straightforward MD at 218 K on s1 (top left) and s2 (bottom left), compared with trajectories obtained at 235 K from RSeeds on s1 (top right) and s2 (bottom right). Gray spheres, purple bonds, and cyan bonds represent surfaces, growing ice, and ice seeds, respectively.

Role of the interfacial water layer

It has been hypothesized that interfacial water plays an important role in heterogeneous ice nucleation. RSeeds method provides an excellent method to test this hypothesis. To this end, we performed several tests to investigate the influence of the interfacial water layer using the RSeeds method.

We first investigated the effect of the choice of the thickness of the interfacial layer, decided by the cutoff in $\rho(z)$ selected in Step 1. In addition to the cutoff used in Sec. Rigid seeding on COOH surface and Rigid seeding on kao_m surface which corresponds to the first hydration layer, we tested configurations with a cutoff that includes the second and third hydration layer on kao_m surface. For each surface configuration, three independent

trajectories are initiated which gives nine trajectories in total. An Ih100 seed with 162 water molecules is used to be consistent with the results obtained at 240 K, and the seed's initial rotation is 0°. At the end of the production run, 8 out of 9 trajectories show seed growth. One seed that is placed after the third hydration layer translates towards the bulk region and dissociates in the production run. This would suggest that the seed is still able to find the rotation and position which results in seed growth with more than one layer of interfacial water. This is particularly beneficial if the surfaces of interest involve roughness, grooves, or surface ions, which require multiple hydration layers for complete coverage. In preliminary results on the mica surface, the thickness of the interfacial water layer plays an important role in determining the fate of the seed. We surmise this is because mica is a poor ice nucleator and has cations on the surface in contact with water.[14] However, we caution that as the seed moves further from the surface, it is less affected by the surface and the surroundings of the seed essentially become bulk liquid. We also emphasize that the rigid seed should be placed in direct contact with the surface with caution. The interfacial water can bridge the rigid seed and surface and is free to adopt any structure that facilitates this. In addition, the harmonic bond and angle potentials applied to maintain the structure of the rigid seed are parameterized in bulk water, and contact with the surface could potentially introduce false configurations at the surface–ice interface.

The second test was performed to investigate the role of mobility of the interfacial water molecules. We used the same kao_m surface with Ih100 seed (162 water molecules and 0 ° initial rotation) and a cutoff corresponding to the first hydration layer in the $\rho(z)$. The only difference between the test case and the RSeeds procedure described in Sec. Rigid seeding on kao_m surface is that the equation of motion for the interfacial water molecules is not integrated, i.e., they are kept frozen for the duration of Step 3. For statistics, we created three different configurations of the interfacial layer with simulations of water on kao_m surface at 300 K. To ensure that the selected configurations are decorrelated we ensured that they are at least 500 ps apart. For each configuration, we initiated three

independent trajectories which give nine trajectories in total. Interestingly, we found that none of the nine seeds found the correct rotation on the kao_m surface, in contrast to the RSeeds where interfacial water was free to move. This test confirms the importance of the mobility of the interfacial water molecules.

The HSEED method uses Random Structure Search (RSS) to mimic the interfacial ice structure. This method has been demonstrated on some test cases.[57] On the s2 surface, the results showed that there are some dissimilarities between the interfacial structures predicted by HSEED and the metadynamics results[28] as well as RSeeds in Sec. Rigid seeding on FCC surfaces. We speculate that one possible cause for this dissimilarity is that the RSS implemented by HSEED assumes the number density of ice on the surface–ice interfacial region is the same as bulk ice. The number density for a layer of Ih100 ice plane is 12.8 nm^{-2} where the number density for the interfacial ice structure on s2 surface is 13.9 nm^{-2}. Although the random perturbation and energy minimization steps in RSS are trying to mimic the interfacial ice structure, it may have difficulty finding the "correct" structure if the water density on the surface is different from the initial seed given. Based on our preliminary results on mica surface, which is a poor ice nucleator, we speculate this issue will be further exacerbated in cases where the surface has roughness, ions, and/or is a weak ice nucleator. RSeeds, on the other hand, avoids this pitfall by using a mobile rigid seed with a layer of interfacial water on the surface, thus allowing the interfacial water to bridge the surface and the seed.

Critical nucleus size and nucleation rate estimates from RSeeds

The critical nucleus size at a specified temperature is the nucleus size at which 50% of the trajectories grow to bulk solid and 50% of the trajectories dissociate to liquid. There are two approaches to identifying the critical nucleus size. In the first approach, crystalline nuclei of constant size are tested at a range of temperatures to identify the temperature at which the seed of the specified size is critical. In the second approach, crystalline seeds

of a range of sizes are tested at a fixed temperature to identify the critical size at that temperature. In both approaches, a number of simulations are initiated from systems comprising solvated crystalline nuclei, and the simulations are continued until the nuclei grow or dissociate.

$\mathbf{Kao_m}$ and TIP4P/Ice

RSeeds was used to identify the critical nucleus size for kao_m at three different temperatures: 237.5, 252.5, and 257.5 K. These temperatures were selected because the homogeneous critical size and nucleation rate at these temperatures are available from previous studies for TIP4P/ice water model.[80] This information is required to estimate the heterogeneous nucleation rate. Moreover, nucleation is accessible in straightforward MD simulations at 237.5 K, thus enabling comparison of RSeeds results with those from straightforward simulations. We make the assumption that the ice polymorph, plane, and rotation do not change within the range of temperatures.

For temperatures at 237.5 and 252.5 K, the starting seed sizes have 42 and 249 water molecules, respectively. The systems are equilibrated for 10 ns at 300 K (Step 3a), annealed to their respective production temperature in 1 ns (Step 3b), and equilibrated at the production temperature (Step 3c) for 50 ns to obtain a wide range of seed sizes. The short annealing time in Step 3b prevents the seed from growing substantially during annealing and allows a collection of a wide range of seed sizes. For 237.5 K, a total of 30 trajectories with 4 different starting seed sizes ranging from 67 to 150 water molecules were used to determine the critical nucleus size. For 252.5 K, a total of 11 configurations with starting seed sizes ranging from 294 to 699 were extracted within 20 ns of Step 3c, and 65 production trajectories were initiated. For temperatures at 257.5 K, 3 starting seed sizes were used: 1280, 1503, and 1965. Each was extracted from a spherical seed with a radius of ~ 3.9 nm, which is the approximate size of a critical nucleus at 257.5 K under homogeneous conditions. Instead of hemispherical seeds which we have been using at stronger supercooling, seeds with smaller contact angles were extracted (see SI for further

information). With Steps 3a and 3b kept the same, the duration for Step 3c was reduced to 10 ns. The dynamics of TIP4P/Ice increase exponentially with temperature, and a long equilibration with rigid seed led to an anisotropically shaped nucleus. To avoid this, we prepared rigid seeds of different sizes and performed shorter equilibration. A total of 68 trajectories with 7 different starting seed sizes ranging from 2152 to 3027 were used to determine the critical nucleus size at 257.5 K.

In order to estimate the nucleation rate and critical nucleus size with straightforward MD at 237.5 K, five simulations of liquid water on kao_m were performed. The kao_m surface size and amount of liquid water on the surface was the same as used in RSeeds. All five trajectories nucleate within 1 μs. Three configurations were extracted from the early stages of crystallization from each of the five nucleation trajectories. Five 50 ns MD simulations are initiated from each configuration.

The procedure to determine the critical nucleus size was the same for RSeeds and straightforward MD. The size of the largest ice cluster was calculated every 10 ps with the $\overline{q}_6$ order parameter described in Sec. Order parameter. To smooth the relatively large fluctuations in seed size for such small seeds, a 500 ps rolling average seed size was calculated. The average seed sizes did not change substantially over the 500 ps window. The starting seed size is reported as the rolling average from the first 500 ps. The upper and lower bounds for classifying growth and dissociation at 237.5, 252.5, and 257.5 K are 200 & 20, 800 & 100, and 4000 & 1000, respectively. That is, at 237.5 K, a trajectory is classified as having grown if the size of the ice cluster exceeds 200, and dissociated if the size falls below 20. Any trajectory in which the seed size fails to cross those boundaries within the production simulation is not counted. The production time for all temperatures is between 50 to 150 ns. Fig. 8 shows the probability of growth with respect to the starting seed size using both methods. The predicted critical nucleus at 237.5, 252.5, and 257.5 K using RSeeds are 72±2, 475±30, and 2510±60, respectively. The critical nucleus size calculated using straightforward MD is 66±5 at 237.5 K. (Refer to SI for error calculation details).

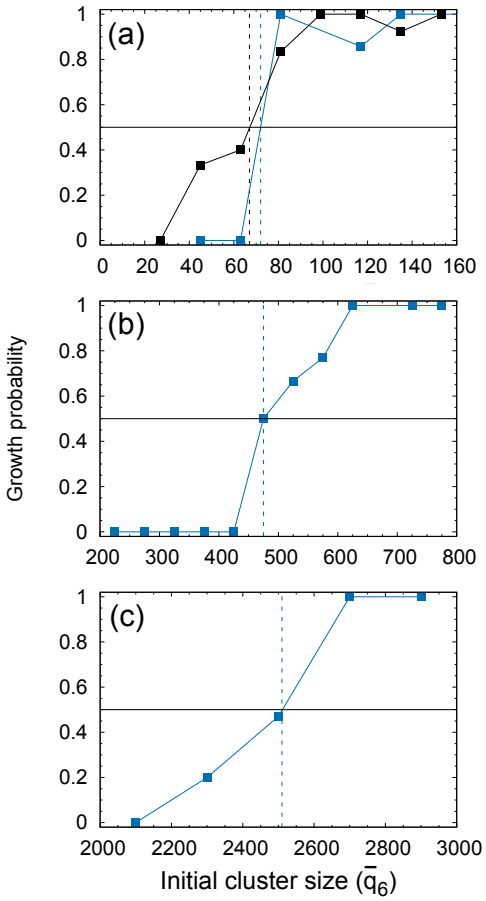

Figure 8: Panel (a)-(c) shows the probability of growth with respect to the initial seed size at 237.5, 252.5, and 257.5 K, respectively. Results from RSeeds and straightforward MD are colored in blue and black, respectively. The critical nucleus is the initial size where the probability of growth is 0.5.

The nucleation rate from straightforward MD at 237.5 K is calculated with the approach outlined by Cox *et al.*[26] The induction time is taken as the time at which the ice cluster size exceeds 200 water molecules. The induction times from the five nucleation trajectories are used to calculate the probability of the system remaining liquid as a function of time. The nucleation rate is extracted by fitting this function to an exponential decay.

Heterogeneous CNT is used to calculate the nucleation rate on the $\mathrm{kao_m}$ surface from RSeeds. The heterogeneous nucleation rate R_{het} can be written as[23,83,84]

$$R_{\mathrm{het}} = A_{\mathrm{het}} \exp\Big[- \frac{f(\theta_c)\Delta G^*_{\mathrm{hom}}}{k_B T} \Big] \tag{1}$$

where A_{het} is the heterogeneous kinetic prefactor, θ_c is the solid–wall contact angle for a critical nucleus, $f(\theta_c)$ is the potency factor, k_{B} is Boltzmann's constant, $\Delta G^*_{\mathrm{hom}}$ is the free energy barrier to form a critical nucleus at temperature T for homogeneous nucleation. The potency factor $f(\theta_c)$ can be expressed as

$$f(\theta_c) = \frac{N_c^{\mathrm{het}}}{N_c^{\mathrm{hom}}} \tag{2}$$

where N_c^{het} and N_c^{hom} are the critical nucleus size for heterogeneous and homogeneous nucleation, respectively. As mentioned at the start of Sec. Results and discussion, this equation is only valid if the N_c^{het} and N_c^{hom} have the same crystal polymorph, in this case, hexagonal ice. For cases where the polymorphs are different, the corrected form can be found in the Supplementary Information of Ref. 28.

If we assume that the heterogeneous kinetic prefactor has the same magnitude as homogeneous,[23] we can write

$$A_{\mathrm{het}} = A_{\mathrm{hom}} = \rho_f f^+ Z \tag{3}$$

where ρ_f is the fluid number density, f^+ is the attachment rate, and Z is the Zeldovich

factor. At a temperature of 237.5 K, $A_{\text{hom}} = 5 \times 10^{37}$ m^{-3}s^{-1}, $N_c^{\text{hom}} = 600$, and $\Delta G^*_{\text{hom}} = 85 \pm 6\ k_{\text{B}}T$ for the water model used in this study.[80] When performing the rate calculation, an error bar of ±10 water molecules for the critical nucleus size predicted by RSeeds is used. However, since we are normalizing N_c^{het} by the homogeneous critical nucleus size, this uncertainty becomes less significant.

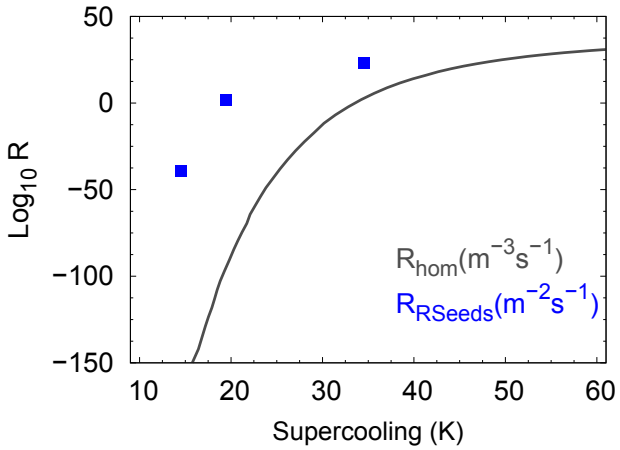

Figure 9: Heterogeneous nucleation rate calculated using RSeeds on modified kaolinite surface. Homogeneous ice nucleation rate is shown as dark gray line and is obtained from Ref. 80.

The rate predicted by heterogeneous CNT is $R_{\text{het}} = 6 \times 10^{32\pm1}$ m^{-3} s^{-1}, comparable to the rate obtained from straightforward simulation, $R_{\text{het,MD}} = 1.2 \times 10^{31}$ m^{-3}s^{-1}. However, expressing the heterogeneous nucleation rate in events per volume per time is non-intuitive since nucleation occurs on the surface rather than in the bulk. Assuming the surface is big enough to eliminate finite size effects,[46] the nucleation rate should be a function of surface area. To express the nucleation rate in terms of area, we write A_{het} as follows:

$$A_{\text{het}} = \rho_{\text{area}} f^+ Z \tag{4}$$

where ρ_{area} is the area density of nucleation sites, defined as the average number of water molecules in the first monolayer per unit area of the surface. The product of the

attachment rate (f^+) and Zeldovich factor (Z) is extracted by dividing the homogeneous prefactor by the bulk water density ($f^+Z = A_{\mathrm{hom}}/\rho_f$). ρ_{area} is calculated from a simulation of water on $\mathrm{kao_m}$ at $\mathrm{T_{prod}}$ prior to nucleation, by dividing the average number of water molecules within the first layer of water on $\mathrm{kao_m}$ by the surface area. The rate calculated using this approach is $R_{\mathrm{het}} = 1 \times 10^{23\pm1}$ m^{-2} s^{-1} and the rate obtained from the straightforward MD is $R_{\mathrm{het,MD}} = 5.6 \times 10^{22}$ m^{-2} s^{-1} at 237.5 K. Both are in reasonable agreement with each other. Therefore, in addition to predicting the correct ice polymorph, plane, and rotation for ice formation on a surface, quantitative estimates of the critical nucleus size and nucleation rate can also be obtained from RSeeds. Based on this, we can also calculate the rate of nucleation at 252.5 K and 257.5 K. Details of the calculations are given in Supplemental Information. The rates calculated are shown in Fig. 9. Indeed, as expected, the nucleation rate on the modified kaolinite surface is higher than homogeneous nucleation rate, and the rate decreases with increasing temperature (i.e, decreasing supercooling). Furthermore, this demonstrates that with RSeeds, we can estimate nucleation rates spanning several orders of magnitude.

FCC surfaces and mW water

The critical nucleus sizes for both s1 and s2 surfaces are estimated using RSeeds at 235 K to compare with the results from metadynamics.[28] For the s1 surface, both Ih001 and Ic111 seeds are used and Ih100 seed is used for the s2 surface. All systems are equilibrated for 10 ns at 300 K (Step 3a), quenched to 235 K, and then equilibrated for 1 ns (Step 3c).

A total of 18 configurations with seed sizes ranging from 120 to 350 are extracted from Step 3c on the s1 surface with an equal spread of Ih001 and Ic111 seeds, and 10 independent trajectories are initiated for each configuration. For the s2 surface, a total of 9 configurations with seed sizes ranging from 54 to 192 were extracted from Step 3c, and 85 trajectories were initiated for the production runs.

In contrast to TIP4P/ice, no upper and lower bounds were used to determine the critical nucleus size for mW water model because the system either grew or dissociated

completely within 2.5 ns. The size of the largest cluster was calculated every 0.5 ps with the q3 order parameter described in Sec. Order parameter, and starting seed size is calculated using the average value of the first 5 ps.

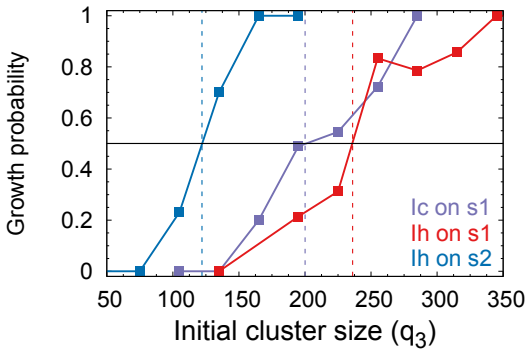

Figure 10: Probability of growth with respect to the initial seed size at 235 K for FCC surfaces. Results for Ic on s1, Ih on s1, and Ih on s2 are colored in purple, red, and blue, respectively. The critical nucleus is the initial size where the probability of growth is 0.5.

From the results shown in Fig. 10, the critical nucleus size for Ic on s1, Ih on s1, and Ih on s2 are 200±34, 236±6, and 122±7, respectively. Since the initial seeds are small, no stacking disordered seed is tested on s1 surface. However, the ice growing from the seeds is mostly stacking disordered. According to metadynamics results, at the same temperature (235 K), the critical nucleus size for the s1 surface is 211 ± 11, and the cluster is stacking disordered with a large percent of Ic.[28] Similarly, the critical nucleus size for the s2 surface is 104 ± 3, and the cluster is completely Ih.[28] The estimates from RSeeds agree well with metadynamics which further validates RSeeds.

The HSEED method predicts the critical nucleus size on the s1 surface[57] to be 330 ± 25 which is roughly 100 water molecules larger than the estimates from metadynamics and RSeeds. As for the s2 surface, the critical nucleus size predicted by HSEED[57] is 290. This corresponds to a discrepancy of >170 water molecules between HSEED and other methods. This difference is significant given the critical nucleus size under homogeneous conditions is <600 at 235 K. From Ref. 57, it can be observed that the rotation of

the best seed on the s1 surface is slightly off compared to the snapshot obtained from metadynamics. We surmise this could cause the disagreement of the critical nucleus size on the s1 surface. One of the reasons for the different critical nucleus sizes on the s2 surface, according to Ref. 57, may stem from the dissimilarities of the interfacial ice structure between HSEED and metadynamics. The possible cause for this dissimilarity has been discussed in Sec. Role of the interfacial water layer.

Conclusions

The strength of RSeeds approach is further enhanced by its potential to be integrated with recent methods developed to study ice. GenIce,[85,86] is a python-based package that allows users to generate different types of ice crystal structures including stacking disordered ice. Thus, GenIce can be used to generate the seeds for use in the RSeeds method. Furthermore, the biased simulation method developed by Naullage et al.[87] can be used in synergy with RSeeds. The ice plane(s) that most favorably bind with the given surface can be identified using the biased simulation method, followed by RSeeds to determine the critical nucleus size and nucleation rate.

RSeeds will enable efficient studies of ice nucleation on surfaces with a range of properties to investigate the mechanism of heterogeneous ice nucleation. It enables one to span a wide range of nucleation rates and therefore, study a broad variety of surfaces including weak ice nucleators. This will build a better understanding of the causal relationship between surface properties and ice nucleation efficiency. Future work includes applying RSeeds to a broad variety of surfaces, including rough surfaces and biological substrates. RSeeds can be easily applied to study heterogeneous crystal nucleation in other systems beyond ice.

Acknowledgement

This material is based upon work supported by NSF CBET #1653352. Clemson University is acknowledged for the generous allotment of compute time on the Palmetto cluster.

Supporting Information Available

Details for the construction of kao_m surface and statistical analysis for seeds rotation on kao_m surface.

References

(1) Murray, B.; O'Sullivan, D.; Atkinson, J.; Webb, M. Ice nucleation by particles immersed in supercooled cloud droplets. *Chem. Soc. Rev.* **2012**, *41*, 6519–6554.

(2) Atkinson, J. D.; Murray, B. J.; Woodhouse, M. T.; Whale, T. F.; Baustian, K. J.; Carslaw, K. S.; Dobbie, S.; O'Sullivan, D.; Malkin, T. L. The importance of feldspar for ice nucleation by mineral dust in mixed-phase clouds. *Nature.* **2013**, *498*, 355.

(3) Christner, B. C.; Morris, C. E.; Foreman, C. M.; Cai, R.; Sands, D. C. Ubiquity of biological ice nucleators in snowfall. *Science.* **2008**, *319*, 1214–1214.

(4) Morris, G. J.; Acton, E. Controlled ice nucleation in cryopreservation–a review. *Cryobiology.* **2013**, *66*, 85–92.

(5) Kobayashi, A.; Golash, H. N.; Kirschvink, J. L. A first test of the hypothesis of biogenic magnetite-based heterogeneous ice-crystal nucleation in cryopreservation. *Cryobiology.* **2016**, *72*, 216–224.

(6) Dalvi-Isfahan, M.; Hamdami, N.; Xanthakis, E.; Le-Bail, A. Review on the control of

ice nucleation by ultrasound waves, electric and magnetic fields. *J. Food Eng.* **2017**, *195*, 222–234.

(7) Hobbs, P. V. *Ice physics*; Oxford classic texts in the physical sciences; Oxford University Press: New York, 2010.

(8) Glatz, B.; Sarupria, S. The surface charge distribution affects the ice nucleating efficiency of silver iodide. *J. Chem. Phys.* **2016**, *145*, 211924.

(9) Zielke, S. A.; Bertram, A. K.; Patey, G. N. Simulations of Ice Nucleation by Model AgI Disks and Plates. *J. Phys. Chem. B.* **2016**, *120*, 2291–2299.

(10) Metya, A. K.; Singh, J. K. Ice Nucleation on a Graphite Surface in the Presence of Nanoparticles. *J. Phys. Chem. C.* **2018**, *122*, 19056–19066.

(11) Roudsari, G.; Reischl, B.; Pakarinen, O. H.; Vehkamäki, H. Atomistic Simulation of Ice Nucleation on Silver Iodide (0001) Surfaces with Defects. *J. Phys. Chem. C.* **2020**, *124*, 436–445.

(12) Soni, A.; Patey, G. N. Unraveling the Mechanism of Ice Nucleation by Mica (001) Surfaces. *J. Phys. Chem. C.* **2021**, *125*, 26927–26941.

(13) Zhou, J.; Lata, N. N.; Sarupria, S.; Cantrell, W. Water Structure on Mica Surfaces: Investigating the Effect of Cations. *ChemRxiv.* **Sep 20, 2019**, 1–15, DOI: 10.26434/chemrxiv.9851975.v1.

(14) Lata, N. N.; Zhou, J.; Hamilton, P.; Larsen, M.; Sarupria, S.; Cantrell, W. Multivalent Surface Cations Enhance Heterogeneous Freezing of Water on Muscovite Mica. *J. Phys. Chem. Lett.* **2020**, *11*, 8682–8689.

(15) Sosso, G. C.; Tribello, G. A.; Zen, A.; Pedevilla, P.; Michaelides, A. Ice formation on kaolinite: Insights from molecular dynamics simulations. *J. Chem. Phys.* **2016**, *145*, 211927.

(16) Sosso, G. C.; Li, T.; Donadio, D.; Tribello, G. A.; Michaelides, A. Microscopic Mechanism and Kinetics of Ice Formation at Complex Interfaces: Zooming in on Kaolinite. *J. Phys. Chem. Lett.* **2016**, *7*, 2350–2355.

(17) Zielke, S. A.; Bertram, A. K.; Patey, G. N. Simulations of ice nucleation by kaolinite (001) with rigid and flexible surfaces. *J. Phys. Chem. B.* **2016**, *120*, 1726–1734.

(18) Glatz, B.; Sarupria, S. Heterogeneous ice nucleation: Interplay of surface properties and their impact on water orientations. *Langmuir.* **2017**, *34*, 1190–1198.

(19) Soni, A.; Patey, G. N. How Microscopic Features of Mineral Surfaces Critically Influence Heterogeneous Ice Nucleation. *J. Phys. Chem. C.* **2021**, *125*, 10723–10737.

(20) Qiu, Y.; Odendahl, N.; Hudait, A.; Mason, R.; Bertram, A. K.; Paesani, F.; DeMott, P. J.; Molinero, V. Ice nucleation efficiency of hydroxylated organic surfaces is controlled by their structural fluctuations and mismatch to ice. *J. Am. Chem. Soc.* **2017**, *139*, 3052–3064.

(21) Sosso, G. C.; Whale, T. F.; Holden, M. A.; Pedevilla, P.; Murray, B. J.; Michaelides, A. Unravelling the origins of ice nucleation on organic crystals. *Chem. Sci.* **2018**, *9*, 8077–8088.

(22) Metya, A. K.; Molinero, V. Is Ice Nucleation by Organic Crystals Nonclassical? An Assessment of the Monolayer Hypothesis of Ice Nucleation. *J. Am. Chem. Soc.* **2021**, *143*, 4607–4624.

(23) Cabriolu, R.; Li, T. Ice nucleation on carbon surface supports the classical theory for heterogeneous nucleation. *Phys. Rev. E.* **2015**, *91*, 052402.

(24) Lupi, L.; Peters, B.; Molinero, V. Pre-ordering of interfacial water in the pathway of heterogeneous ice nucleation does not lead to a two-step crystallization mechanism. *J. Chem. Phys.* **2016**, *145*, 211910.

(25) Zhang, C.; Wang, Y.; Wang, J.; Zhou, X. Size of Nanoscale Domains in Inhomogeneous Surfaces Determines Ice Nucleation. *J. Phys. Chem. C.* **2022**, *126*, 13373–13380.

(26) Cox, S. J.; Kathmann, S. M.; Slater, B.; Michaelides, A. Molecular simulations of heterogeneous ice nucleation. I. Controlling ice nucleation through surface hydrophilicity. *J. Chem. Phys.* **2015**, *142*, 184704.

(27) Cox, S. J.; Kathmann, S. M.; Slater, B.; Michaelides, A. Molecular simulations of heterogeneous ice nucleation. II. Peeling back the layers. *J. Chem. Phys.* **2015**, *142*, 184705.

(28) Fitzner, M.; Sosso, G. C.; Pietrucci, F.; Pipolo, S.; Michaelides, A. Pre-critical fluctuations and what they disclose about heterogeneous crystal nucleation. *Nat. Commun.* **2017**, *8*, 2257.

(29) Pedevilla, P.; Fitzner, M.; Michaelides, A. What makes a good descriptor for heterogeneous ice nucleation on OH-patterned surfaces. *Phys. Rev. B.* **2017**, *96*, 115441.

(30) Haji-Akbari, A.; DeFever, R. S.; Sarupria, S.; Debenedetti, P. G. Suppression of sub-surface freezing in free-standing thin films of a coarse-grained model of water. *Phys. Chem. Chem. Phys.* **2014**, *16*, 25916–25927.

(31) Molinero, V.; Moore, E. B. Water modeled as an intermediate element between carbon and silicon. *J. Phys. Chem. B.* **2008**, *113*, 4008–4016.

(32) Torrie, G. M.; Valleau, J. P. Nonphysical sampling distributions in Monte Carlo free-energy estimation: Umbrella sampling. *J. Comput. Phys.* **1977**, *23*, 187–199.

(33) Laio, A.; Parrinello, M. Escaping free-energy minima. *Proc. Natl. Acad. Sci. U.S.A.* **2002**, *99*, 12562–12566.

(34) Barducci, A.; Bussi, G.; Parrinello, M. Well-tempered metadynamics: a smoothly converging and tunable free-energy method. *Phys. Rev. Lett.* **2008**, *100*, 020603.

(35) Peters, B.; Trout, B. L. Obtaining reaction coordinates by likelihood maximization. *J. Chem. Phys.* **2006**, *125*, 054108.

(36) Peters, B.; Beckham, G. T.; Trout, B. L. Extensions to the likelihood maximization approach for finding reaction coordinates. *J. Chem. Phys.* **2007**, *127*, 034109.

(37) Li, C.; Liu, Z.; Goonetilleke, E. C.; Huang, X. Temperature-dependent kinetic pathways of heterogeneous ice nucleation competing between classical and non-classical nucleation. *Nat. Commun.* **2021**, *12*, 4954.

(38) Allen, R. J.; Warren, P. B.; ten Wolde, P. R. Sampling rare switching events in biochemical networks. *Phys. Rev. Lett.* **2005**, *94*, 018104.

(39) Allen, R. J.; Frenkel, D.; ten Wolde, P. R. Simulating rare events in equilibrium or nonequilibrium stochastic systems. *J. Chem. Phys.* **2006**, *124*, 024102.

(40) Hall, S. W.; Grisell, D. L.; Sarupria, S.; Rogal, J. Practical guide to replica exchange transition interface sampling and forward flux sampling. *J Chem. Phys.* **2022**, *156*, 200901.

(41) Li, T.; Donadio, D.; Russo, G.; Galli, G. Homogeneous ice nucleation from supercooled water. *Phys. Chem. Chem. Phys.* **2011**, *13*, 19807–19813.

(42) Reinhardt, A.; Doye, J. P. K. Free energy landscapes for homogeneous nucleation of ice for a monatomic water model. *J. Chem. Phys.* **2012**, *136*, 054501.

(43) Lupi, L.; Hudait, A.; Peters, B.; Grünwald, M.; Mullen, R. G.; Nguyen, A. H.; Molinero, V. Role of stacking disorder in ice nucleation. *Nature.* **2017**, *551*, 218.

(44) Borrero, E. E.; Escobedo, F. A. Reaction coordinates and transition pathways of rare events via forward flux sampling. *J. Chem. Phys.* **2007**, *127*, 164101.

(45) Lupi, L.; Hanscam, R.; Qiu, Y.; Molinero, V. Reaction coordinate for ice crystallization on a soft surface. *J. Chem. Phys. Lett.* **2017**, *8*, 4201–4205.

(46) Hussain, S.; Haji-Akbari, A. How to quantify and avoid finite size effects in computational studies of crystal nucleation: The case of heterogeneous ice nucleation. *J. Chem. Phys.* **2021**, *154*, 014108.

(47) Hussain, S.; Haji-Akbari, A. Role of Nanoscale Interfacial Proximity in Contact Freezing in Water. *J. Am. Chem. Soc.* **2021**, *143*, 2272–2284.

(48) Abascal, J. L. F.; Sanz, E.; García Fernández, R.; Vega, C. A potential model for the study of ices and amorphous water: TIP4P/Ice. *J. Chem. Phys.* **2005**, *122*, 234511.

(49) Haji-Akbari, A.; Debenedetti, P. G. Direct calculation of ice homogeneous nucleation rate for a molecular model of water. *Proc. Natl. Acad. Sci. USA.* **2015**, *112*, 10582–10588.

(50) Bai, X.-M.; Li, M. Test of classical nucleation theory via molecular-dynamics simulation. *J. Chem. Phys.* **2005**, *122*, 224510.

(51) Bai, X.-M.; Li, M. Calculation of solid-liquid interfacial free energy: A classical nucleation theory based approach. *J. Chem. Phys.* **2006**, *124*, 124707.

(52) Espinosa, J. R.; Vega, C.; Valeriani, C.; Sanz, E. Seeding approach to crystal nucleation. *J. Chem. Phys.* **2016**, *144*, 034501.

(53) Zimmermann, N. E. R.; Vorselaars, B.; Espinosa, J. R.; Quigley, D.; Smith, W. R.; Sanz, E.; Vega, C.; Peters, B. NaCl nucleation from brine in seeded simulations: Sources of uncertainty in rate estimates. *J. Chem. Phys.* **2018**, *148*, 222838.

(54) Espinosa, J. R.; Sanz, E.; Valeriani, C.; Vega, C. Homogeneous ice nucleation evaluated for several water models. *J. Chem. Phys.* **2014**, *141*, 18C529.

(55) Sanchez-Burgos, I.; Sanz, E.; Vega, C.; R., E. J. Fcc vs. hcp competition in colloidal hard-sphere nucleation: on their relative stability, interfacial free energy and nucleation rate. *Phys. Chem. Chem. Phys.* **2021**, *23*, 19611–19626.

(56) Lamas, C. P.; Espinosa, J. R.; Conde, M. M.; Ramírez, J.; Montero de Hijes, P.; Noya, E. G.; Vega, C.; Sanz, E. Homogeneous nucleation of NaCl in supersaturated solutions. *Phys. Chem. Chem. Phys.* **2021**, *23*, 26843–26852.

(57) Pedevilla, P.; Fitzner, M.; Sosso, G. C.; Michaelides, A. Heterogeneous seeded molecular dynamics as a tool to probe the ice nucleating ability of crystalline surfaces. *J. Chem. Phys.* **2018**, *149*, 072327.

(58) Pedevilla, P.; Fitzner, M.; Sosso, G. C.; Michaelides, A. Heterogeneous seeded molecular dynamics as a tool to probe the ice nucleating ability of crystalline surfaces. *J. Chem. Phys.* **2018**, *149*, 072327.

(59) Lupi, L.; Hudait, A.; Molinero, V. Heterogeneous nucleation of ice on carbon surfaces. *J. Am. Chem. Soc.* **2014**, *136*, 3156–3164.

(60) Lupi, L.; Molinero, V. Does hydrophilicity of carbon particles improve their ice nucleation ability? *J. Phys. Chem. A.* **2014**, *118*, 7330–7337.

(61) Li, C.; Tao, R.; Luo, S.; Gao, X.; Zhang, K.; Li, Z. Enhancing and Impeding Heterogeneous Ice Nucleation through Nanogrooves. *J. Phys. Chem. C.* **2018**, *122*, 25992–25998.

(62) Li, C.; Gao, X.; Li, Z. Surface Energy-Mediated Multistep Pathways for Heterogeneous Ice Nucleation. *J. Phys. Chem. C.* **2018**, *122*, 9474–9479.

(63) Kiselev, A.; Bachmann, F.; Pedevilla, P.; Cox, S. J.; Michaelides, A.; Gerthsen, D.; Leisner, T. Active sites in heterogeneous ice nucleation—the example of K-rich feldspars. *Science.* **2017**, *355*, 367–371.

(64) Fitzner, M.; Sosso, G. C.; Cox, S. J.; Michaelides, A. The many faces of heterogeneous ice nucleation: Interplay between surface morphology and hydrophobicity. *J. Am. Chem. Soc.* **2015**, *137*, 13658–13669.

(65) Pedevilla, P.; Cox, S. J.; Slater, B.; Michaelides, A. Can ice-like structures form on non-ice-like substrates? The example of the K-feldspar microcline. *J. Phys. Chem. C.* **2016**, *120*, 6704–6713.

(66) Zaragoza, A.; Conde, M. M.; Espinosa, J. R.; Valeriani, C.; Vega, C.; Sanz, E. Competition between ices Ih and Ic in homogeneous water freezing. *J. Chem. Phys.* **2015**, *143*, 134504.

(67) Wang, J.; Wolf, R. M.; Caldwell, J. W.; Kollman, P. A.; Case, D. A. Development and testing of a general amber force field. *J. Comput. Chem.* **2004**, *25*, 1157–1174.

(68) Jorgensen, W. L.; Maxwell, D. S.; Tirado-Rives, J. Development and testing of the OPLS all-atom force field on conformational energetics and properties of organic liquids. *J. Am. Chem. Soc.* **1996**, *118*, 11225–11236.

(69) Love, J. C.; Estroff, L. A.; Kriebel, J. K.; Nuzzo, R. G.; Whitesides, G. M. Self-assembled monolayers of thiolates on metals as a form of nanotechnology. *Chem. Rev.* **2005**, *105*, 1103–1170.

(70) Wang, H.; Chen, S.; Li, L.; Jiang, S. Improved method for the preparation of carboxylic acid and amine terminated self-assembled monolayers of alkanethiolates. *Langmuir.* **2005**, *21*, 2633–2636.

(71) Cygan, R. T.; Liang, J. J.; Kalinichev, A. G. Molecular models of hydroxide, oxyhydroxide, and clay phases and the development of a general force field. *J. Phys. Chem. B.* **2004**, *108*, 1255–1266.

(72) Abraham, M. J.; Murtola, T.; Schulz, R.; Páll, S.; Smith, J. C.; Hess, B.; Lindahl, E. GROMACS: High performance molecular simulations through multi-level parallelism from laptops to supercomputers. *SoftwareX.* **2015**, *1*, 19–25.

(73) Essmann, U.; Perera, L.; Berkowitz, M. L.; Darden, T.; Lee, H.; Pedersen, L. G. A smooth particle mesh Ewald method. *J. Chem. Phys.* **1995**, *103*, 8577.

(74) Miyamoto, S.; Kollman, P. A. Settle: An analytical version of the SHAKE and RATTLE algorithm for rigid water models. *J. Comput. Chem.* **1992**, *13*, 952–962.

(75) Hess, B.; Bekker, H.; Berendsen, H. J. C.; Fraaije, J. G. E. M. LINCS: a linear constraint solver for molecular simulations. *J. Comput. Chem.* **1997**, *18*, 1463–1472.

(76) Plimpton, S. Fast parallel algorithms for short-range molecular dynamics. *J. Comput. Phys.* **1995**, *117*, 1–19.

(77) Bussi, G.; Donadio, D.; Parrinello, M. Canonical sampling through velocity rescaling. *J. Chem. Phys.* **2007**, *126*, 014101.

(78) Berendsen, H. J. C.; Postma, J. P. M.; van Gunsteren, W. F.; DiNola, A.; Haak, J. R. Molecular dynamics with coupling to an external bath. *J. Chem. Phys.* **1984**, *81*, 3684–3690.

(79) Lechner, W.; Dellago, C. Accurate determination of crystal structures based on averaged local bond order parameters. *J. Chem. Phys.* **2008**, *129*, 114707.

(80) Espinosa, J. R.; Sanz, E.; Valeriani, C.; Vega, C. Homogeneous ice nucleation evaluated for several water models. *J. Chem. Phys.* **2014**, *141*, 18C529.

(81) Sanz, E.; Vega, C.; Espinosa, J. R.; Caballero-Bernal, R.; Abascal, J. L. F.; Valeriani, C. Homogeneous ice nucleation at moderate supercooling from molecular simulation. *J. Am. Chem. Soc.* **2013**, *135*, 15008–15017.

(82) Sun, Y.; Song, H.; Zhang, F.; Yang, L.; Ye, Z.; Mendelev, M. I.; Wang, C.; Ho, K. Overcoming the time limitation in Molecular Dynamics simulation of crystal nucleation: a persistent-embryo approach. *Phys. Rev. Lett.* **2018**, *120*, 085703.

(83) Turnbull, D. Formation of crystal nuclei in liquid metals. *J. Appl. Phys.* **1950**, *21*, 1022–1028.

(84) Turnbull, D. Kinetics of heterogeneous nucleation. *J. Chem. Phys.* **1950**, *18*, 198–203.

(85) Matsumoto, M.; Yagasaki, T.; Tanaka, H. GenIce: Hydrogen-Disordered Ice Generator. *J. Comput. Chem.* **2018**, *39*, 61–64.

(86) Doi, H.; Takahashi, K. Z.; Aoyagi, T. Mining of Effective Local Order Parameters to Classify Ice Polymorphs. *J. Phys. Chem. A.* **2021**, *125*, 9518–9526.

(87) Naullage, P. M.; Metya, A. K.; Molinero, V. Computationally efficient approach for the identification of ice-binding surfaces and how they bind ice. *J. Chem. Phys.* **2020**, *153*, 174106.